Proceedings of the Symposium A of the European Materials Research, Warsaw, September 2008

Fabrication and Raman Studies of MgO/SnO_2 Core-Shell Heteronanowires

H.S. Kim and H.W. Kim*

Division of Materials Science and Engineering, Inha University

Incheon 402–751, Republic of Korea

We have reported the fabrication of MgO core/SnO_2 shell nanowires, by a two-step evaporation process. Thermal annealing induced changes in morphology, in which the nanowire surface became rough by the agglomeration of SnO_2 shell layers and its crystallinity was enhanced. It was found that three fundamental modes (475, 634, 772 cm^{-1}) and an infrared (IR)-active mode (682 cm^{-1}) of rutile SnO_2 appeared in the Raman spectrum of MgO core/SnO_2 shell nanowires. By thermal annealing, the relative intensity of the A_{2u} to the A_{1g} line was reduced, presumably due to the disorder or size effects.

PACS numbers: 81.07.−b, 78.30.−j, 61.05.cp

1. Introduction

Since magnesium oxide (MgO) is a typical wide bandgap insulator, the electronic and the optical properties of bulk MgO have been intensively studied [1–3]. In addition, MgO is a very important material for use in catalysis, toxic waste remediation, refractory, paint and superconductors [4–6]. On the other hand, tin oxide (SnO_2) is an n-type semiconductor with a wide band gap ($E_g = 3.6$ eV at 300 K). It is well known for its potential applications in gas sensors [7], transparent conducting electrodes [8], transistors [9], and solar cells [10].

Heterostructures of one-dimensional (1D) nanowires have been intensively studied, since they are promising materials for applications as nanodevices owing to their small dimensions and novel properties. Accordingly, many researchers have prepared the heteronanowires by various methods. Since both MgO and SnO_2 have the extraordinary physical and chemical properties, we expect that nanowire heterostructures consisting of these materials will provide a variety of applications such as nanoscale optoelectronics, sensors, and catalysts, etc.

In this paper, we have demonstrated the fabrication of MgO core/SnO_2 shell nanowires, in which a two-step evaporation technique has been used. With the thermal heating/annealing being inevitable in the ULSI fabrication process for the fabrication of nanodevices, we have investigated the effect of annealing on the morphology, crystallinity, and Raman properties.

2. Experimental

For preparing the core MgO nanowires, pure MgB_2 powders were heated at 900°C in the ambient gas (Ar + O_2) [11]. The products were deposited on gold (Au)-coated Si substrates located inside a quartz tube. In order to fabricate the MgO core/SnO_2 shell nanowires, we have used the evaporation method with Sn powders. On top of the alumina boat with the Sn powders, a piece of the MgO nanowires-grown substrate was placed with the deposition side downwards. In the heating process at 900°C, the typical percentages of O_2 and Ar partial pressure, respectively, were set to approximately 3 and 97%. In the subsequent step, for some selected samples, a thermal annealing was performed in a quartz tube at 800°C for 10 min.

We have characterized the samples by using a glancing angle (0.5°) X-ray diffraction (XRD, X'pert MPD-Philips with Cu K_{α_1} radiation) with the contribution from the substrate being minimized, scanning electron microscopy (SEM, Hitachi S-4200), and transmission electron microscopy (TEM, Philips CM-200) equipped with an energy-dispersive X-ray (EDX) spectroscopy. Micro-Raman spectra were obtained using a Renishaw Raman spectromicroscope scanning from 100 cm^{-1} to 1200 cm^{-1} at room temperature in an open air. An He–Ne laser beam with a wavelength of 633 nm was used for the Raman excitation.

3. Results and discussion

Figure 1a shows a typical SEM image of as-prepared MgO core/SnO_2 shell nanowires, exhibiting the 1D nature of the products. We have carried out EDX measurements in conjunction with TEM investigation. Figures 1b and c show the elemental maps of Mg and Sn elements, respectively, for an MgO core/SnO_2 shell nanowire. While Mg elements mainly reside in the central (core) region, Sn elements are extensively present in the outer region, as well as in the core region. Figure 1d is an associated selected area electron diffraction

* corresponding author; e-mail: hwkim@inha.ac.kr

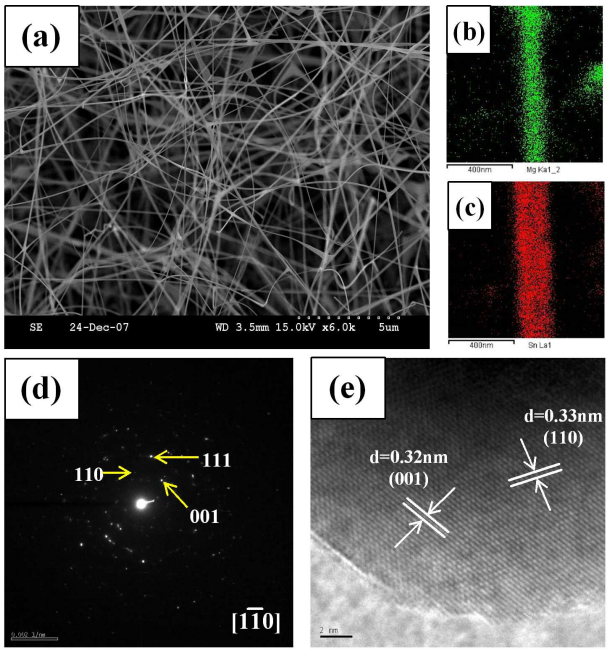

Fig. 1. (a) SEM image of as-prepared MgO core/SnO_2 shell nanowires. TEM–EDX elemental maps of (b) Mg and (c) Sn elements for a core-shell nanowire. (d) Associated EDX pattern. (e) Lattice-resolved TEM image near the surface of a core-shell nanowire.

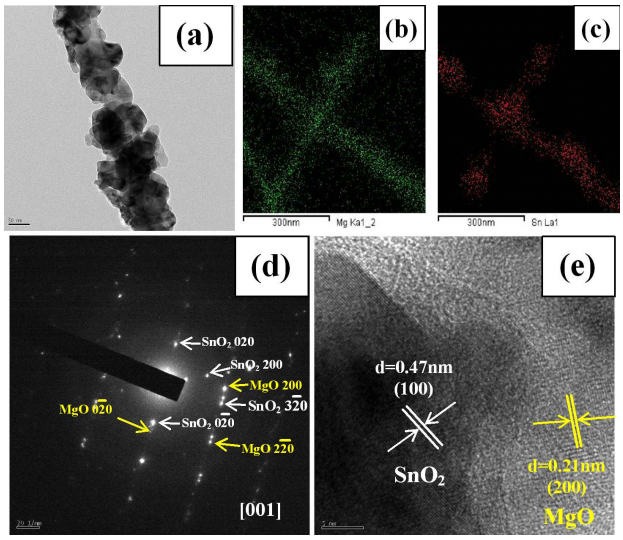

Fig. 2. (a) TEM image of an annealed MgO core/SnO_2 shell nanowires. TEM–EDX elemental maps of (b) Mg and (c) Sn elements for two crossed core-shell nanowires. (d) Associated EDX pattern. (e) Lattice-resolved TEM image.

(SAED) pattern, confirming the existence of tetragonal SnO_2 phase. Figure 1e shows a lattice-resolved TEM image enlarging an area near the nanowire surface. It shows the spacing of 0.32 nm and 0.33 nm between two neighbouring layers, corresponding to d_{001} and d_{110} spacing of tetragonal SnO_2, respectively.

Figure 2a shows a SEM image of MgO core/SnO_2 shell nanowires, which were annealed at 800°C. It is observed that the surface of heteronanowires became rough by the thermal annealing. Figures 2b and c show the elemental maps of Mg and Sn elements, respectively, for two crossed MgO core/SnO_2 shell nanowires. The Mg elements were present everywhere in the heteronanowires, whereas Sn elements were apparently localized. From Figs. 2a–c, we notice that the SnO_2 shell layers have been agglomerated by the thermal annealing. The SAED pattern of the core-shell nanowire (Fig. 2d) shows an overlap of two sets of diffraction spots, corresponding to a cubic MgO structure and a tetragonal SnO_2 structure, respectively. In order to investigate in detail, we have carried out the high-resolution TEM analysis. As shown in Fig. 2a, the annealed core-shell nanowires consist of dark and bright regions, respectively. Figure 2e shows a lattice-resolved TEM image enlarging a boundary between the dark and bright regions. For the bright region on the right-hand-side of Fig. 2e, the measured d spacing is 0.21 nm in accordance with (002) plane of cubic MgO. On the other hand, the dark region on the left-hand side of Fig. 2e shows an interplanar spacing of 0.47 nm, which corresponds to the (100) lattice plane of tetragonal SnO_2 structure. Accordingly, we deduce that the SnO_2 shell layers were agglomerated to form a cluster-like structure, with some part of MgO core being exposed.

Figure 3a shows an XRD pattern of core MgO nanowires prior to SnO_2 coating, revealing that the whole spectrum can be indexed in peak position to a cubic MgO phase (JCPDS: 04-0829). Figures 3b and c show XRD patterns of as-prepared and 800°C-annealed MgO core/SnO_2 shell nanowires, respectively. It is noteworthy that the heteronanowires mainly exhibited a tetragonal rutile structure of SnO_2 (JCPDS File No. 41-1445). XRD peak-broadening analysis was performed for Figs. 3b and c, in which the relatively strong diffraction peaks corresponding to the (110), (101), and (211) indices of SnO_2 were extracted. The full-width-at-half-maximum (FWHM) values of the (110) peak, (101) peak, and (211) peak in the unannealed samples are about 0.34°, 0.30°, and 0.38°, respectively (Fig. 4). On the other hand, the FWHM values of the (110), (101), and (211) peaks in the annealed samples are approximately 0.30°, 0.26°, and 0.30°, respectively (Fig. 4). Accordingly, the SnO_2--associated peaks became sharper and thus the SnO_2 grain size became larger by the thermal annealing [12]. Accordingly, the overall degree of crystallization of the SnO_2 shell was increased after a thermal annealing.

Figure 5a shows the room-temperature Raman spectrum of the core MgO nanowires. While the sharp peak at 520 cm^{-1} was identified as the TO phonon mode in the silicon (Si) crystal structure [13], presumably from the Si substrates, the peak centered at 939 cm^{-1} is associated with the surface phonon mode of amorphous silica, which should have been formed on the surface of Si sub-

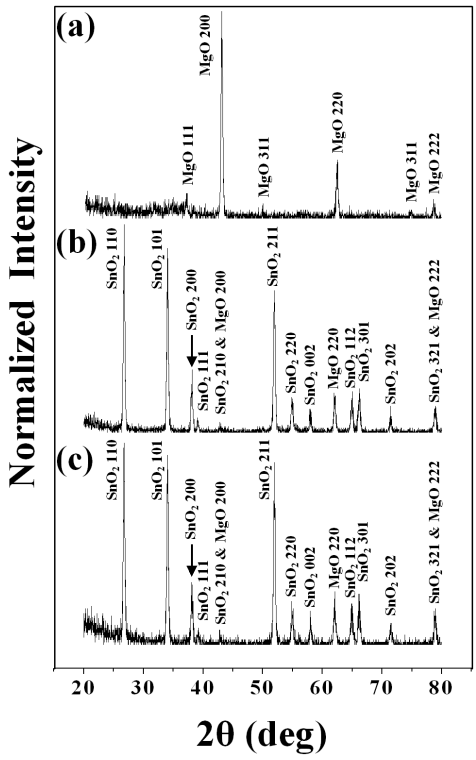

Fig. 3. XRD patterns of (a) MgO core nanowires, (b) the as-prepared MgO core/SnO_2 shell nanowires, (c) the annealed MgO core/SnO_2 shell nanowires.

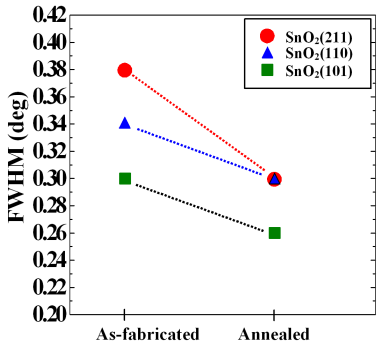

Fig. 4. FWHM values of SnO_2(211), SnO_2(110), and SnO_2(101) diffraction peaks for as-prepared and annealed MgO core/SnO_2 shell nanowires.

strate [14]. The Raman lines at 290 cm^{-1} and 448 cm^{-1} may coincide with the two prominent peaks in Chen's calculation in regard to MgO microcrystals [15, 16]. Accordingly, it is supposed that the 290 cm^{-1} line is associated with a TA phonon at the zone boundary, whereas 448 cm^{-1} line with a TO phonon at the zone center. In addition, the line at 1080 cm^{-1} accompanied by line at 1121 cm^{-1} is observed. This rather broad band composed of two lines is similar to those observed from MgO microcrystals [15, 17], being ascribed to the surface phonon modes in a TO–LO phonon gap.

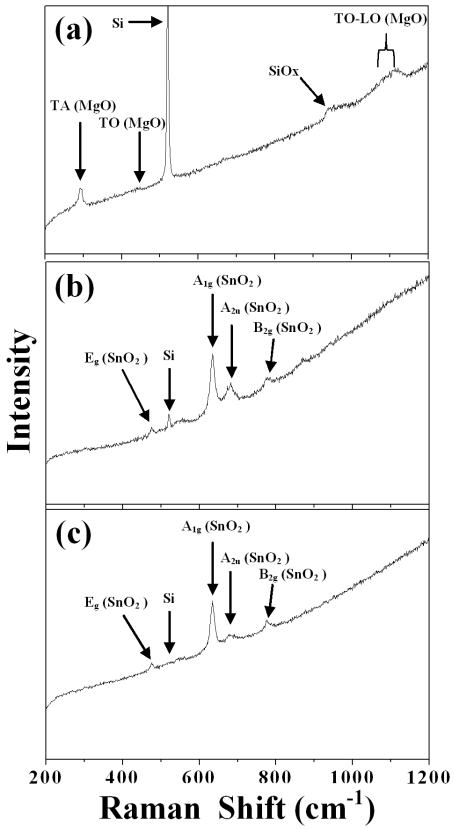

Fig. 5. Room-temperature Raman spectra of (a) MgO core nanowires, (b) the as-prepared MgO core/SnO_2 shell nanowires, (c) the annealed MgO core/SnO_2 shell nanowires.

Figure 5b shows the Raman spectrum of the as--prepared MgO core/SnO_2 shell nanowires. By comparing with Fig. 5a, we notice that TA phonon- and TO--phonon-related Raman lines are not clearly observed. Furthermore, the Raman lines of the TO–LO phonon gap were significantly suppressed. It is noteworthy that the 520 cm^{-1} line from Si has been significantly reduced in its relative intensity. Accordingly, we suggest that the Raman peaks from core MgO nanowires as well as Si substrates have been significantly suppressed, presumably due to the covering effect by the shell layer. Three normal interior phonon modes, E_g, A_{1g}, and B_{2g}, which usually appear in large single crystals or bulk polycrystalline SnO_2 materials, are detected at frequencies of 475, 634, and 772 cm^{-1}, respectively [18–20], confirming the tetragonal rutile structure of the SnO_2 shell layers. Additionally, the Raman forbidden line at 682 cm^{-1} was observed, which can be assigned to the IR-active LO A_{2u} mode of SnO_2 [18, 19]. Figure 5c shows the Raman spectrum of the 800°C-annealed MgO core/SnO_2 shell nanowires. Being similar to the unannealed sample (Fig. 5b), the Raman spectrum of annealed sample apparently exhibits E_g, A_{1g}, B_{2g}, and A_{2u} lines from SnO_2, whereas MgO-related lines are not clearly observed.

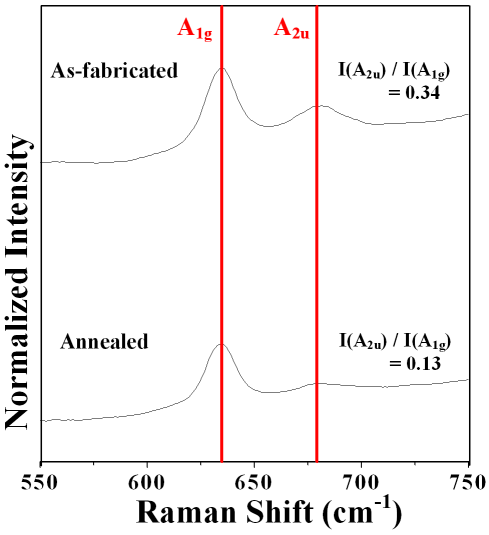

Fig. 6. Raman spectra of MgO core/SnO_2 shell nanowires, which were as-prepared and annealed, respectively, in the range of 550–750 cm^{-1}.

In order to investigate the effect of thermal annealing in more detail, the Raman spectra of the MgO core/SnO_2 shell nanowires with a Raman shift in the range of 550–750 cm^{-1} are displayed in Fig. 6. In order to remove the meaningless noises, we have plotted smoothed spectra. We note that the relative intensity of the IR-active LO A_{2u} mode line to the A_{1g} line was reduced by the thermal annealing. The Raman activity of the IR-active LO A_{2u} mode line could be induced by a disorder [19] or size effects [21]. Accordingly, we surmise that the thermal annealing tended to decrease the disorder by increasing the crystallinity of SnO_2 samples. The other possibility is that the IR-active mode, which had been induced by the size effect of the thinner thickness of the shell layer, became suppressed by the annealing--induced agglomeration of shell layers. Further study is in progress.

4. Conclusions

By heating Sn powders onto the as-grown MgO nanowires, MgO core/SnO_2 shell nanowires were successfully fabricated. TEM investigation revealed that the SnO_2 shell layer became agglomerated with the MgO surface being exposed. XRD patterns indicated that the SnO_2-associated peaks became sharper and thus the SnO_2 grain size became larger by the thermal annealing. The Raman spectrum of MgO core/SnO_2 shell nanowires exhibits three fundamental modes (E_g, A_{1g}, B_{2g}) of rutile SnO_2, as well as the IR-active A_{2u} mode. The relative intensity of the A_{2u} mode line to the A_{1g} line was reduced by the thermal annealing.

Acknowledgments

The work was supported by Inha University Research Grant.

References

[1] G.P. Summers, T.M. Wilson, B.T. Jeffries, H.T. Tohver, Y. Chen, M.M. Abraham, *Phys. Rev. B* **27**, 1283 (1983).

[2] G.H. Rosenblatt, M.W. Rowe, G.P. Williams, Jr., R.T. Williams, Y. Chen, *Phys. Rev. B* **39**, 10309 (1989).

[3] J.L. Grant, R. Cooper, P. Zeglinski, J.F. Boas, *J. Chem. Phys.* **90**, 807 (1989).

[4] S.H.C. Liang, I.D. Gay, *J. Catal.* **101**, 293 (1986).

[5] A.N. Copp, *Am. Ceram. Soc. Bull.* **74**, 135 (1995).

[6] P.D. Yang, C.M. Lieber, *Science* **273**, 1836 (1996).

[7] J. Watson, *Sens. Actuators* **5**, 29 (1984).

[8] Y.S. He, J.C. Campbell, R.C. Murphy, M.F. Arendt, J.S. Swinnea, *J. Mater. Res.* **8**, 3131 (1993).

[9] G. Sberveglieri, *Sens. Actuators* **6**, 64 (1992).

[10] S. Ferrere, A. Zaban, B.A. Gregg, *J. Phys. Chem. B* **101**, 4490 (1997).

[11] H.W. Kim, S.H. Shim, *Chem. Phys. Lett.* **422**, 165 (2006).

[12] B.D. Cullity, *Elements of X-ray Diffraction*, Addison--Wesley, Massachusetts 1978.

[13] M. Hirasawa, T. Orii, T. Seto, *Appl. Phys. Lett.* **88**, 093119 (2006).

[14] Y.D. Glinka, M. Jaroniec, *J. Appl. Phys.* **82**, 3499 (1997).

[15] K. Ishikawa, N. Fujima, H. Komura, *J. Appl. Phys.* **57**, 973 (1985).

[16] T.S. Chen, F.W. de Wette, L. Kleinman, D.G. Dempsey, *Phys. Rev. B* **17**, 844 (1978).

[17] H.K. Böckelmann, R.G. Schlecht, *Phys. Rev. B* **10**, 5225 (1974).

[18] Y. Liu, M. Liu, *Adv. Funct. Mater.* **15**, 57 (2005).

[19] L. Abello, B. Bochu, A. Gaskov, S. Koudryavtseva, G. Lucazeau, M. Roumyantseva, *J. Solid State Chem.* **135**, 78 (1998).

[20] A. Dieguez, A. Romano-Rodriguez, A. Vila, R. Morante, *J. Appl. Phys.* **90**, 1550 (2001).

[21] X.P. Peng, L.D. Zhang, G.W. Meng, Y.T. Tian, Y. Lin, B.Y. Geng, S.H. Sun, *J. Appl. Phys.* **93**, 1760 (2003).